Modified potential-induced-breathing model of potentials between close-shell ions

Huoyi Zhang and M. S. T. Bukowinski
Department of Geology and Geophysics, University of California at Berkeley, Berkeley, California 94720
(Received 1 March 1991)

We have developed a simple *ab initio* model for the calculation of the thermoelastic properties of ionic compounds. The model is based on the Gordon-Kim-type electron-gas theory with spherically symmetric relaxation of ionic charge densities. The relaxation is controlled by a spherically averaged potential due to the total crystal charge density. The potential is self-consistent with the charge distribution, and contains Coulomb, exchange, and correlation contributions. We find that this potential yields anions that are slightly smaller than those stabilized by a point-ion Coulomb potential only. In the case of MgO, this results in a zero-pressure density that differs from experiment by less than 1%, a significant improvement over models that include only point-ion stabilization potentials. Further, the calculated equations of state and $B1$-$B2$ phase-transition pressures of NaCl, KCl, MgO, CaO, and SrO are in equally good agreement with data. The calculated equation of state and structure of the more covalent and less symmetric SiO_2 stishovite is only slightly less accurate.

I. INTRODUCTION

The cubic oxides, especially MgO and CaO, and the high-pressure phases of SiO_2 are of considerable geophysical interest and have been subjected to intensive theoretical and experimental scrutiny. Much effort[1-4] has been devoted in recent years to model the thermoelastic properties of oxide minerals with electron-gas theories of ionic interactions. These are approximate quantum mechanical models which can be easily extended to complex minerals and have shown much promise in modeling mineral thermoelastic properties under the extreme conditions of planetary interiors.

In 1972 Gordon and Kim[5] developed the electron-gas theory of crystals of closed-shell ions. They approximated the total charge density of a crystal ρ as a sum of ionic/atomic charges which were assumed to be rigid and spherically symmetric. The overlap interactions were given by electrostatic, kinetic, exchange, and correlation energy functionals of ρ. The atomic or ionic charge distributions were derived from self-consistent Hartree-Fock (HF) wave functions. The electron-gas energy functionals (strictly valid only for a uniform and infinite electron gas) tend to underestimate the total kinetic energy, and overestimate the exchange and correlation energies Waldman and Gordon[6] introduced scaling factors which ensured an approximate agreement between the atomic energies computed from the Hartree-Fock and electron-gas methods. Although the modified electron-gas (MEG) model has achieved some success with simple oxides, it did not prove sufficiently accurate for a quantitative description of crystal thermoelastic properties. The model tends to underestimate the zero pressure density and, as all rigid-ion models, cannot account for the observed violation of the Cauchy relations.

To overcome the rigid-ion problem, Muhlhausen and Gordon[7] introduced a shell-stabilized MEG (SSMEG) model which allows the ionic charge distribution to contract, or expand, in response to a Watson-sphere-potential[8] approximation to the crystal point-ion Coulomb potential. The atomic charge distributions were derived from the Hartree-Fock equation with the Watson sphere potential included as an external potential. Boyer *et al.*[9] introduced a similar model, the potential-induced-breathing (PIB) model, which also allows the ionic charge distributions to spherically distort in response to the electrostatic site potential. Instead of the Hartree-Fock equation, the latter authors used a density functional approximation to the Dirac equation to compute the ionic charge densities. Since the atomic charge distributions deform under crystal strain, both SSMEG and PIB models include ionic self-energy contributions to the crystal energy.

The PIB model has been used to examine the high-pressure properties of several oxides, including MgO, CaO, SrO, and BaO,[1] corundum and stishovite[2] and $MgSiO_3$ perovskite.[3] In most cases, reasonably good agreement between theoretical predictions and experimental data was achieved. Stishovite, which is presumably more covalent than the cubic oxides, did not fare as well. A notable success of the PIB model is its ability to yield elastic constants that violate the Cauchy relations in the manner observed in the cubic oxides.

In an attempt to further increase the accuracy of electron-gas potentials, Wolf and Bukowinski[4] required that the total crystal energy be minimized with respect to the Watson sphere radius. Electronic charge densities were again computed with the Hartree-Fock equation. The anion charge densities thus obtained are more sensitive to crystal structure and, in contrast to the PIB and earlier models, depend on the chemical composition of the crystal. Some improvement in the accuracy of the equations of state and elastic constants of MgO and CaO were obtained.

No attempt was made in any of these models to make the charge density self-consistent with the crystal potential. Complete self-consistency requires an appropriate band-structure calculation. It is, however, possible to re-

tain the advantages of a pair-potential model, and achieve a good measure of self-consistency, by requiring that the spherical ionic charge densities be consistent with the corresponding total crystal potential. We present here an approximation to this ideal in which the ionic densities are made self-consistent with the spherically averaged crystal potential around the ionic site. The crystal potential is based on the same Hamiltonian as that used to obtain the ionic densities, and includes approximate exchange and correlation effects, as well as Coulomb interactions. We show that excellent agreement is thus obtained with the experimental equations of state and $B1$-$B2$ phase transformation pressures of cubic ion compounds. We also achieve significant improvements in the calculated equation of state and structure of SiO_2 stishovite.

We begin by outlining, in Sec. II, the theoretical approach and calculation methods. In Sec. III the predicted compression curve and phase transition of oxides are presented. As a further test of the model, the calculated equations of state and phase transition pressures of NaCl and KCl are also presented in this section. Sec. IV summarizes the results.

II. DESCRIPTION OF MODEL

A. Total energy calculation

Our model is based on the Gordon-Kim-type electron-gas theory. The crystal is assumed to consist of overlapping spherical ions or atoms. The total crystal energy per unit cell U contains of the long-range Coulomb energy, the overlap energy, and the self-energy; i.e.,

$$U=U_{\text{Madelung}}+U_{\text{overlap}}+U_{\text{self}} . \tag{1}$$

The Madelung energy, U_{Madelung}, is calculated with the Ewald[10] method. U_{self} contains self-energy contributions ϕ_α from each ion in the unit cell

$$U_{\text{self}}=\sum_\alpha \phi_\alpha . \tag{2}$$

ϕ_α is the energy of the ion subjected to the crystal potential, measured relative to a reference state, to be defined later. Within the pairwise approximation, the total overlap energy can be expressed in the form

$$U_{\text{overlap}}=\tfrac{1}{2}\sum{}'\phi_{\alpha\beta}(R) , \tag{3}$$

where R is the interatomic distance and α and β range over all ions in the cell and all ions in the crystal, respectively. The prime on the summation indicates that the $\alpha=\beta$ terms are omitted. The overlap pair interaction $\phi_{\alpha\beta}(R)$ contains electrostatic, kinetic, exchange, and correlation-energy contributions,

$$\phi_{\alpha\beta}=\phi^e_{\alpha\beta}+\phi^k_{\alpha\beta}+\phi^x_{\alpha\beta}+\phi^c_{\alpha\beta} . \tag{4}$$

The short-range electrostatic interaction energy $\phi^e_{\alpha\beta}$ results from the overlap of the charge distributions of ions α and β, and can be expressed in terms of their respective charge distributions, ρ_α and ρ_β, and their nuclear and ionic charges, Z_α and Q_α:

$$\phi^e_{\alpha\beta}(R)=\frac{Z_\alpha Z_\beta-Q_\alpha Q_\beta}{R}\int d\mathbf{r}_1\int d\mathbf{r}_2\frac{\rho_\alpha(\mathbf{r}_1)\rho_\beta(\mathbf{r}_2)}{r_{12}} -Z_\beta\int d\mathbf{r}_1\frac{\rho_\alpha(\mathbf{r}_1)}{r_{1\beta}}-Z_\alpha\int d\mathbf{r}_2\frac{\rho_\beta(\mathbf{r}_2)}{r_{2\alpha}} \tag{5}$$

where r_{12}, $r_{1\beta}$, and $r_{2\alpha}$ are electron-1–electron-2, electron-1–nucleus-β, and electron-2–nucleus-α distances, respectively.

The non-Coulombic overlap interactions ($\phi^k_{\alpha\beta},\phi^x_{\alpha\beta},\phi^c_{\alpha\beta}$) are approximated with local density functionals:

$$\phi^\Gamma_{\alpha\beta}=\int d\mathbf{r}[\rho_{\alpha\beta}\varepsilon^\Gamma(\rho_{\alpha\beta})-\rho_\alpha\varepsilon^\Gamma(\rho_\alpha)-\rho_\beta\varepsilon^\Gamma(\rho_\beta)] , \tag{6}$$

where $\rho_{\alpha\beta}=\rho_\alpha+\rho_\beta$, and Γ stands for k, x, or c. The Thomas-Fermi functional, without correction parameters, is used to approximate the kinetic-energy density ε^k and the combined exchange-correlation energy density $[\varepsilon^x(\rho)+\varepsilon^c(\rho)]$ is estimated with the Hedin-Lundqvist model.[11] The summation of short-range pair interactions in Eq. (3) is extended to the fourth nearest neighbors in crystals with $B1$ symmetry, and fifth nearest neighbors in those with $B2$ symmetry. For ion pairs at separations greater than twice the nearest-neighbor distance the overlap contributions are negligible.

B. Self-consistent crystal potential and charge distributions

The ionic charge densities (ρ_α) are given by $\rho=\sum_i n_i|\Psi_i|^2$, where n_i is the number of electrons in ith orbital and Ψ_i is a solution of

$$(H+V_{\text{crystal}})\Psi_i=E_i\Psi_i , \tag{7}$$

where H is the Hamiltonian operator[12] of a free ion, with the Hedin-Lundqvist parametrization of the exchange-correlation energy, E_i is the orbital energy, and V_{crystal} is the potential due to all other atoms in the crystal.

V_{crystal} contains Coulomb, V^c_{crysal}, and exchange-correlation, V^{xc}_{crystal} contributions:

$$V_{\text{crystal}}=V^c_{\text{crystal}}+V^{xc}_{\text{crystal}} . \tag{8}$$

If we let the ion whose charge is to be computed to the 0th ion, then V^c_{crystal} is given by

$$V^c_{\text{crystal}}(\mathbf{x})=\int d\mathbf{x}'\sum_{i\neq 0}\frac{Z_i\delta(|\mathbf{x}'-\mathbf{R}_i|)-\rho_i(|\mathbf{x}'-\mathbf{R}_i|)}{|\mathbf{x}-\mathbf{x}'|} . \tag{9}$$

$\mathbf{R}_i$ and $\mathbf{x}$ (or $\mathbf{x}'$) are the coordinates of the ith ion and an electron, respectively, as measured from the 0th ion. As in the free-ion Hamiltonian, the Hedin-Lundqvist model is used to represent v^{xc}_{crystal}.

For computational ease, we use an approximation to V_{crystal} that is similar to a Watson-sphere potential. Inside a sphere of radius ξ, we replace V_{crystal} with its spherical average $\langle V_{\text{crystal}}\rangle$, which is then approximated by a polynomial of the distance from the ion's center. Outside the sphere, the potential is assumed to be of the form $-Q^*/r$. The radius is chosen such that $\langle V_{\text{crystal}}\rangle(\xi)=-Q^*/\xi$, where Q^* is the electronic

TABLE I. Effective charges on anion sites in crystals.

Compound	NaCl	KCl	MgO	CaO	SrO
$B1$ structure	0.78	1	1.72	1.8	2
$B2$ structure	0.86	1	1.64	1.8	2

charge of the 0th ion that lies outside a sphere of radius at which the spherical average of the total crystal potential is a maximum. Q^* changes little with compression and we therefore take it to be independent of pressure for a given composition and structure.

A starting V_{crystal} is obtained from ionic charge densities calculated with Watson-sphere stabilizing potentials, as is done to obtain PIB potentials.[9] New ionic charge densities are then obtained from Eq. (7), and the process is repeated until ξ changes by less than 10^{-4} atomic units. We find that this yields a good measure of self-consistenty of the ionic charge distribution. The procedure usually requires from five to eight iterations.

Sample crystal potentials of O^{2-} in MgO in the $B1$ structure are shown in Fig. 1. Values of Q^* are listed in Table I. Shown for comparison are the corresponding Watson-sphere-type potentials, defined as

$$V_{\text{Watson}}=\begin{cases}-Q/r_{\text{Madelung}}, & \text{for } r\le r_{\text{Madelung}},\\ -Q/r, & \text{for } r>r_{\text{Madelung}},\end{cases}$$

where $Q=2$ for O^{2-} ion, and $r_{\text{Madelung}}=d/a_{\text{Madelung}}$, where d is the nearest-neighbor distance and a_{Madelung} the Madelung constant. Note that overlap effects make V_{crystal} at the O^{2-} site in MgO ($B1$) more attractive than the Watson-sphere potential inside the ionic sphere. As pressure increases ionic overlap, so does the difference between V_{crystal} and V_{Watson}.

C. Cohesive energy

The cohesive energy of alkali halides equals the total crystal energy at zero pressure if the self-energy is referenced to that of a free ion. However, Eq. (7) with the Hedin-Lundqvist Hamiltonian often does not yield stable negative ions. We therefore reference the self-energy of Cl^- ions to their energy in a sufficiently expanded crystal, as obtained by increasing the lattice constant of an alkali-chloride crystal until an asymptotic value of the Cl^- energy is found. This ionic energy is $-458.437\,78$ a.u.

Since the free O^{2-} ion does not exist in nature we calculate the cohesive energy of the alkaline-earth oxides according to

$$\text{MO(solid)}=M^{2+}\text{(free ion)}+\text{O}^-\text{(free ion)}+e^-$$

for M=Mg, Ca, and Sr. The Hartree-Fock energy difference of the reaction

$$\text{O}^{2-}(g,V;{}^1S)\rightarrow\text{O}^-(g;{}^2P)+e^-$$

is $-0.352\,21$ a.u.,[13] where g stands for the ground state and V the stabilizing potential which yields the limit value of the HF energy. We use the HF energy of $O^{2-}(g,V;{}^1S)$ ($-74.437\,30$ a.u.) as the self-energy reference for total-energy calculations. After adding an estimated correlation-energy difference between $O^-(g;{}^2P)$ and $O^{2-}(g;{}^1S)$, the reaction energy for the process is -0.269 ± 0.011 a.u.[13] We calculate the cohesive energy by subtracting the correlation-energy difference and the reaction energy from the calculated binding energy.

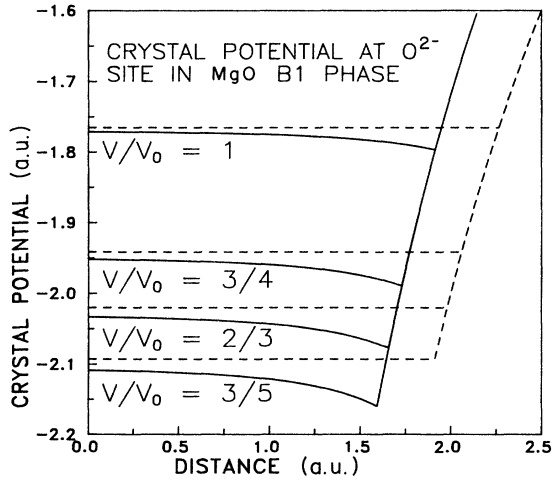

FIG. 1. Crystal potentials at O^{2-} site in MgO ($B1$ structure) at different V/V_0 ratios. Solid lines are from our calculations. Dashed lines are from the Madelung potential with the Watson-sphere approximation.

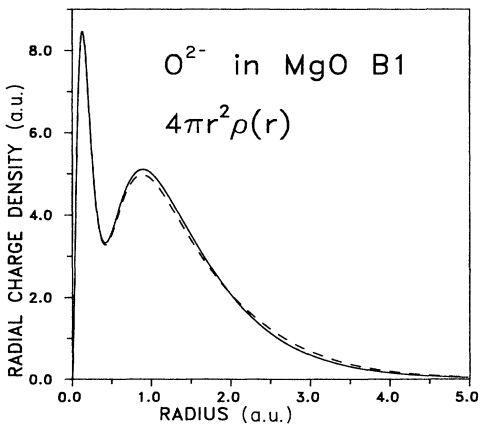

FIG. 2. Radial charge densities of O^{2-} in MgO ($B1$ structure) at zero pressure. The solid line is derived from our crystal potential model. The dashed line is derived from the Madelung potential with the Watson-sphere approximation.

D. Equations of state

We calculate the equations of state $P(V)$ from the standard thermodynamic relation, $P(V)=-(\partial F/\partial V)_T$, where the Helmholtz free energy per unit cell $F(V,T)$ is the sum of the static lattice energy $U(V)$, the zero-point vibrational free energy $F_0(V)$, and the thermal free energy, $F_{th}(V,T)$:

$$F(V,T)=U(V)+F_0(V)+F_{th}(V,T)\ . \tag{10}$$

We use the Debye model to approximate the zero-point free energy and the thermal free energy. The Debye temperature Θ and the Grüneisen parameter γ, are estimated from the static lattice energy $U(V)$ according to a model described by Aidun and Bukowinski.[14] Pressures at which the $B1$ (NaCl structure) phase transforms to the $B2$ (CsCl) phase are obtained by equating the corresponding Gibbs free energies $G(P,T)=F+PV$.

III. RESULTS

A. Charge densities

The zero-pressure radial charge densities of O^{2-} and Mg^{2+} ions in a MgO $B1$ structure are shown in Figs. 2 and 3. where they are compared to the corresponding densities derived from the Watson-sphere potentials. $V_{crystal}$ yields anions that are slightly smaller, but makes no discernible difference to the Mg^{2+} charge distribution. The smaller O^{2-} ion yields a denser crystal than that predicted by the PIB model. The static lattice constant at zero pressure is reduced from 4.3 Å of the PIB model to 4.19 Å. We find that O^{2-} is more compressible in our

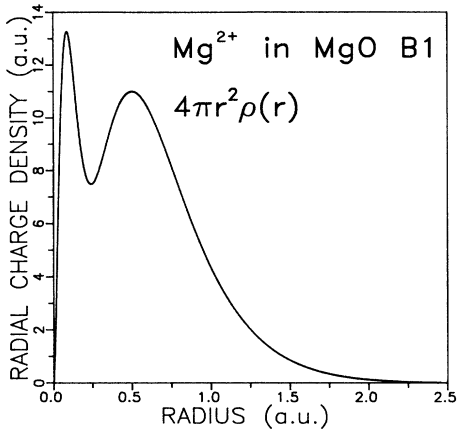

FIG. 3. Radial charge densities of Mg^{2+}. On the scale of the graph, the density obtained from the crystal potential is indistinguishable from that obtained with a Watson-sphere approximation to the Coulomb potential.

TABLE II. Thermodynamic properties of NaCl and KCl.

	Static properties			Room-tempeature properties				
Compound/ structure data/model	Lattice constant D_0 (Å)	Bulk modulus K_0 (GPa)	Cohesive energy E (eV)	Volume at 0 Pa V_0 (Å^3)	Bulk modulus K (GPa)	K'	Debye temperature Θ (K)	Grüneisen parameter γ
NaCl ($B1$)								
our model	5.571	28.08	7.97	44.85	24.30	4.93	314	1.59
data	5.64[a,b]		8.03[b]	44.85[c]	23.8(75)[d]	4.0(39)[d]	308[e]	1.62[f]
SSMEG model	5.64[15]	32.0[b]	7.98[b]					
NaCl ($B2$)								
our model	3.420	37.31	7.67	41.02	34.4	4.36	357	1.33
data				41.7(27)[d,g]	36.2(42)[d,g,h]	4[d,g,h]		
SSMEG model	3.000[b]		7.67[b]					
KCl ($B1$)								
our model	6.200	19.35	7.40	62.04	16.27	5.16	238	1.68
data			7.35[i]	62.42[c]	17.45[c]	5.23[c]	230[j]	
EG model	6.10[i]	22.5[i]	7.60[i]					
KCl ($B2$)								
our model	3.717	26.86	7.30	52.93	23.86	4.82	274	1.55
data				51.87[g,h,k]	31.6[g,h,k]	4[g,h,k]		
EG model	3.636[i]		7.49[i]					

[a]Value at $T=0$ K.
[b]Reference 15.
[c]Reference 16.
[d]Reference 17.
[e]Calculated from thermal expansivity.
[f]Reference 34.
[g]High-pressure data extrapolated to $P=0$.
[h]Assuming $K'=4$.
[i]Reference 5.
[j]Calculated from thermal expensivity.
[k]Reference 19.

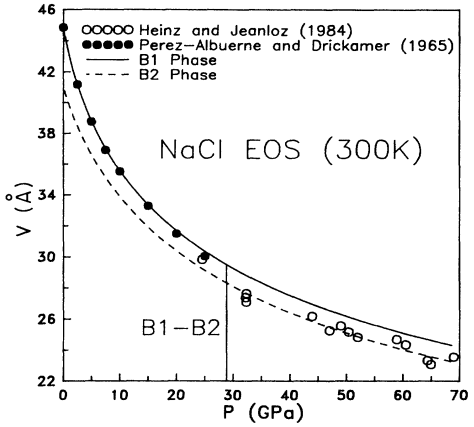

FIG. 4. NaCl equation of state at 300 K. The solid and dashed lines are the theoretical equations of state of the $B1$ or $B2$ structures, respectively. The solid and open circles are data (Refs. 16 and 17). The vertical line, $B1$-$B2$, indicates the predicted phase-transition pressure at 300 K.

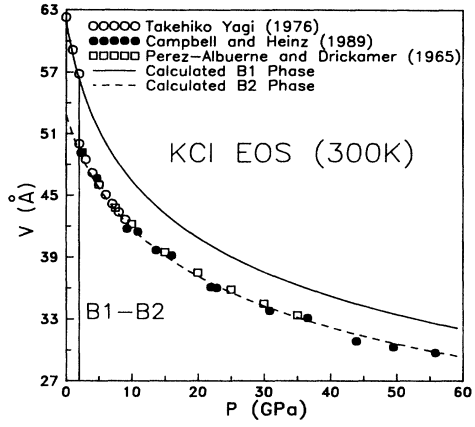

FIG. 5. KCl equation of state at 300 K. Meaning of lines is the same as in Fig. 4. The solid and open circles and open squares are data (Refs. 18, 19, and 16).

model than in the PIB model at the pressures examined here.

B. Equations of state and phase transitions of cubic ion crystals

The equilibrium properties of KCl and NaCl and their structural stabilities are calculated to test the model. The equilibrium properties at 300 K are listed in Table II. The results from some previous electron-gas calculations[15] are also listed for comparison. Figures 4 and 5 compare our calculations with the experimental equations of state at room temperature from Perez-Albuerne and Drickamer,[16] and Yagi,[18] and the recent high-pressure measurements of Campbell and Heinz.[19] Phase-transition pressures from $B1$ to $B2$ structures are listed in Table III, with experimental data also listed for comparison.[16,17] The calculated phase-transition pressures of both materials are in excellent agreement with the data.

The calculated equilibrium properties of the alkaline-earth oxides, MgO, CaO, and SrO are compared with data in Table IV, along with results from other electron-gas calculations.[1] The improvement in the predicted thermodynamic properties due to the self-consistent treatment of the crystal potential is apparent. Figures 6–8 show the calculated and experimental equations of state at room temperature. Our calculations are in excellent agreement with measurements of volume at all pressures, with deviations not exceeding experimental uncertainties. A Birch-Murnaghan fit to the calculated equation of state of MgO yields a bulk modulus of 180 GPa, which is higher than the acoustically determined value of 163 GPa. However, the calculated equation of state of MgO agrees very well with the equation of state obtained from static compression measurements.

The phase-transition pressures from $B1$ to $B2$ structures are listed in Table V, with experimental data also listed for comparison.[16,20–24] The calculated phase-transition pressures of CaO and SrO are in good agreement with the data. The predicted $B1$-$B2$ phase-transition pressure of MgO is 580 GPa; there is no re-

TABLE III. Phase-transition pressure and volume change.

Compound		NaCl[a]	KCl[b]
$B1$-$B2$ transition	This study	29	2.1
pressure (GPa)	Data	29(3)	2.0
Volume change (Å^3)	This study	−1.20	−6.91
Volume change (%)	This study	−4	−12
	Data	−1.3[c]	
		−5.8[d]	

[a]Data from Ref. 17.
[b]Data from Ref. 16.
[b]Heinz and Jeanloz in Ref. 17.
[d]Sato-Sorensen in Ref. 17.

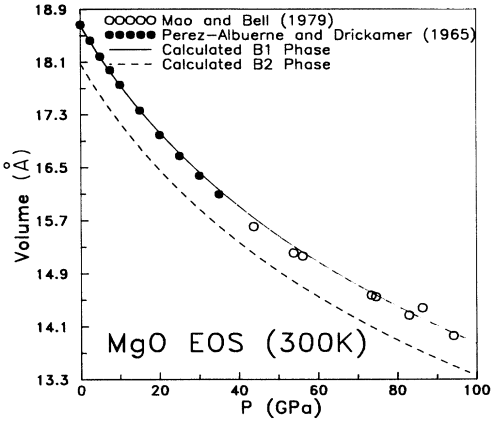

FIG. 6. MgO equation of state at 300 K. Meaning of the lines is the same as in Fig. 4. The solid and open circles are data (Refs. 16 and 20).

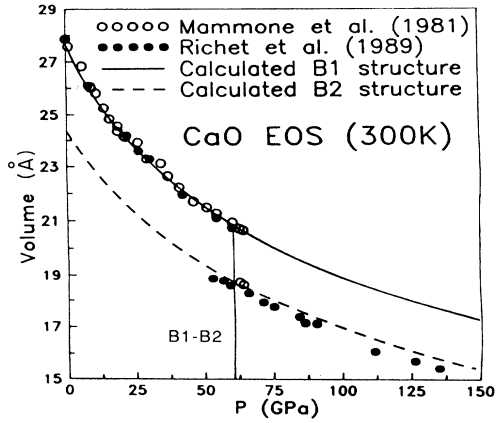

FIG. 7. CaO equation of state at 300 K. Meaning of lines is the same as in Fig. 4. The solid and open circles are data (Refs. 22 and 21).

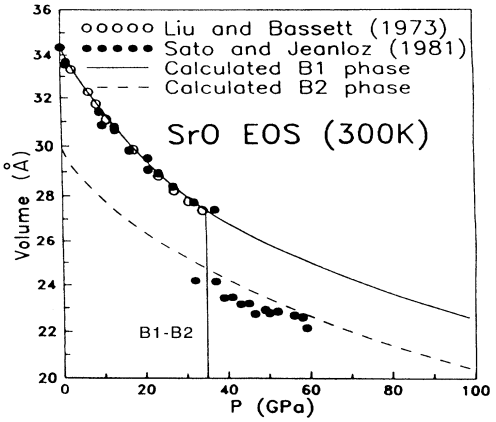

FIG. 8. SrO equation of state at 300 K. Meaning of lines is the same as in Fig. 4. The solid and open circles are data (Refs. 24 and 23).

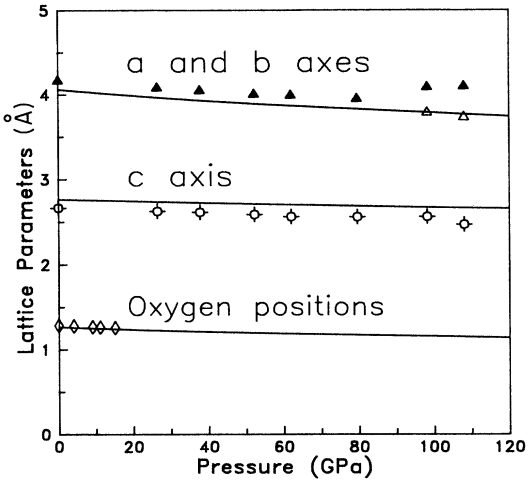

FIG. 9. Pressure dependence of stishovite structural parameters. Data on (a) solid triangles, (b) open triangles, and (c) are from Tsuchida and Yagi (Ref. 28). The absolute oxygen position is the product of a and u parameters and the data are from Ross, Shu, Hazen, and Gasparik (Ref. 30).

ported observation of any transition up to the highest experimental pressure of 200 GPa.[33]

C. SiO_2 stishovite

The structural properties of SiO_2 stishovite were obtained by minimizing the Gibbs free energy with respect to the structural parameters of an orthorhombic unit cell. There are five parameters: three lattice constants: a, b, and c, and two oxygen coordinates in units of a and b, respectively, u and v. In the case of tetragonal rutile structure, $a = b$ and $u = v$.

Because a fully numerical self-consistent calculation

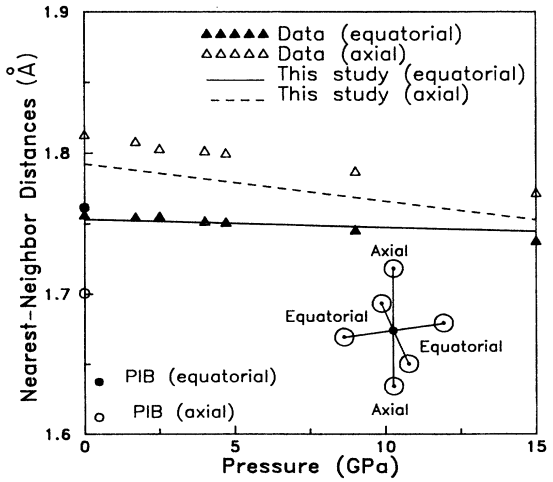

FIG. 10. Si—O bond lengths of stishovite. Data are from Ross *et al.* (Ref. 30).

TABLE IV. Thermodyanmic properties of MgO, CaO, and SrO.

Compound/ structure data/model	Static properties: Lattice constant D_0 (Å)	Static properties: Bulk modulus K_0 (GPa)	Static properties: Cohesive energy E (eV)	Room-temperature properties: 0 pressure volume V_0 (Å^3)	Room-temperature properties: Bulk modulus K (GPa)	Room-temperature properties: K'	Room-temperature properties: Debye temperature Θ (K)	Grüneisen parameter γ
MgO ($B1$)								
Our model	4.192	187	31.9	18.65	180	4.04	837	1.24
Data			31.4[a]	18.67[b]	163[c]	4.13(9)[c]	776[d]	1.5[d]
PIB model	4.30	139	33.5					
MgO ($B2$)								
Our model	2.613	182	30.5	18.07	175	4.20	830	1.26
CaO ($B1$)								
Our model	4.800	121	28.3	27.96	118	4.08	660	1.22
data			27.4[a]	27.82[f]	111(2)[g]	4.2(2)[g]	605[d]	1.5[d]
PIB model	4.82	102	30.1					
CaO ($B2$)								
Our model	2.890	140	27.5	24.45	136	4.26	704	1.29
Data[b]				24.59(33)[g]	130(20)[g]	3.5(5)[g]		
SrO ($B1$)								
Our model	5.159	93.4	26.8	34.72	91	4.19	551	1.30
Data			25.6[b]	34.35[i]	91.3(27)[i]	4.3(3)[i]		
PIB model[e]	5.13	80						
SrO ($B2$)								
Our model	3.090	130	25.9	29.79	128	4.08	637	1.23
Data[h]				28.13[j,k]	160(19)[j,k]	4.0[j,k]		

[a]Reference 13.
[b]Reference 25.
[c]Reference 26.
[d]Reference 27.
[e]Reference 1.
[f]Reference 21.
[g]Reference 22.
[h]Obtained from high-pressure fits, i.e., extrapolated to $P=0$.
[i]Reference 23.
[j]Assumes $K'=4$.
[k]Reference 24.

TABLE V. Phase-transition pressure and volume change.

Compound		MgO[a]	CaO[b]	SrO[c]
$B1$-$B2$ transition	This study	580	61	35
pressure (GPa)	Data	>200	63(4)	36(4)
Volume change (Å^3)	This study	−0.31	−2.09	−2.70
	Data		−2.0	−3.4
Volume change (%)	This study	−3.4	−10	−10
	Data		−10.0	−13.0

[a]Data from Ref. 20
[b]Data from Ref. 21.
[c]Data from Ref. 24.

TABLE VI. Zero-pressure properties of stishovite.

Properties	This study	Experiment	PIB Model
Volume (Å)	45.54	46.54	43.39
c/a ratio	0.681	0.638	0.708
u	0.311	0.306	0.306
K_0 (GPa)	378	287∼313[a]	411
K_0'	6.4±3.5	1.7–6[a]	3.73

[a]References 30–32.

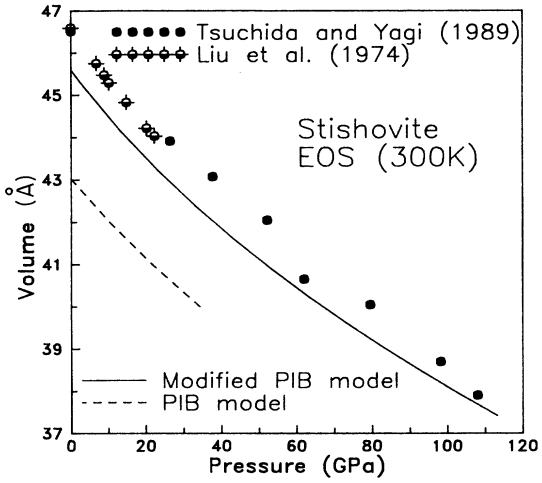

FIG. 11. Stishovite equation of state. The solid line is from our model and the dashed line is from PIB model. Data from Liu, Bassett, and Takahashi (Ref. 29) and Tsuchida and Yagi (Ref. 28).

like the ones employed for the cubic compounds is too time consuming on a minicomputer, we fit the pair potentials to functions of the distance r_{ij} between ions i and j:

$$V(r_{ij}) = \sum_{k=1}^{5} A_k \left[\frac{A_6}{r_{ij}^{5/3}} \right]^k . \tag{11}$$

The A_k's were constrained by fitting Eq. (11) to self-consistent pair potentials for 30 sets of orthorhombic structural parameters that span the range expected in the energy minimization. We found that the 30 sets of A_k's thus obtained can be accurately described by third-order polynomials in the Coulomb energy per molecule.

The model stishovite remains in the tetragonal rutile structure up to 150 GPa. A structural change from the tetragonal rutile structure to an orthorhombic $CaCl_2$ structure was recently observed at approximately 100 GPa in a static compression experiment.[28]

Figure 9 shows that the pressure dependence of the crystal parameters is in good agreement with the data.[28,30] The octahedral bond lengths shown in Fig. 10 have the same trends with pressure as the data.[30] The structural and equation-of-state parameters together with data[30–32] and the results[2] of PIB model calculations are listed in Table VI. The equation-of-state results are compared to data in Fig. 11. The self-consistency requirement clearly yields a significant improvement in the accuracy of the calculated structure and equation of state of stishovite. However, the agreement is not as good as found for the cubic ionic crystals, suggesting that covalent effects are significant in stishovite. Another likely source of error is the low coordination of the oxygen ion in stishovite, which may render the spherical approximation to the potential less than adequate.

IV. SUMMARY

A modified potential-induced-breathing (MPIB) model has been developed to improve the accuracy of electron-gas-type potentials. The relaxation of the ionic charge density is controlled by a spherically averaged potential that is obtained from simple density functional theory. The potential is self-consistent with a crystalline superposition of spherical ionic charge distributions, and contains Coulomb, exchange, and correlation contributions. We find that with this potential anions are more sensitive to their environment than in models where the charge density responds only to the point-ion Coulomb potential of the crystal. Significant improvements are obtained for calculated thermodynamic properties of cubic oxide compounds and SiO_2 stishovite.

[1]M. J. Mehl, R. J. Hemley, and L. L. Boyer, Phys. Rev. B **33**, 8685 (1986).
[2]R. Cohen, Geophys. Res. Lett. **14**, 37 (1987).
[3]R. Cohen, Geophys. Res. Lett. **14**, 1053 (1987).
[4]G. H. Wolf and M. S. T. Bukowinski, in *High-Pressure Research in Mineral Physics,* edited by M. H. Manghnani and Y. Syono (Terra Scientific Publishing Company and American Geophysical Union, Washington, 1987), p. 313.
[5]R. G. Gordon and Y. S. Kim, J. Chem. Phys. **56**, 3122 (1972); Y. S. Kim and R. G. Gordon, Phys. Rev. B **9**, 3548 (1974).
[6]M. Waldman and R. G. Gordon, J. Chem. Phys. **71**, 1353 (1979).
[7]C. Muhlhausen and R. G. Gordon, Phys. Rev. B **23**, 900 (1981); **24**, 2147 (1981).
[8]R. Watson, Phys. Rev. **111**, 1108 (1958).
[9]L. L. Boyer, M. J. Mehl, M. J. Feldman, J. R. Hardy, J. W. Flocken, and C. Y. Fong, Phys. Rev. Lett. **54**, 1940 (1985).
[10]P. P. Ewald, Ann. Phys. (Leipzig) **64**, 253 (1921).
[11]L. Hedin and B. I. Lundqvist, J. Phys. C **4**, 2064 (1971).
[12]F. Herman and S. Skillman, *Atomic Structure Calculations* (Prentice-Hall, Englewood Cliffs, NJ, 1963).
[13]A. J. Cohen and R. G. Gordon, Phys. Rev. B **14**, 4593 (1976).
[14]J. Aidun and M. S. T. Bukowinski, Phys. Rev. B **29**, 2611 (1984).
[15]R. J. Hemley and R. G. Gordon, J. Geophys. Res. **90**, 7803 (1985).
[16]E. A. Perez-Albuerne and H. G. Drickamer, J. Chem. Phys. **43**, 1381 (1965).
[17]D. L. Heinz and R. Jeanloz, Phys. Rev. B **30**, 6045 (1984); Y. Sato-Sorensen, J. Geophys. Res. **88**, 3543 (1983).
[18]T. Yagi, ISSP report, 1976 (unpublished).
[19]A. J. Campbell and D. L. Heinz, EOS **43**, 1356 (1989).
[20]H. K. Mao and P. M. Bell, J. Geophys. Res. **84**, 4533 (1979).
[21]J. F. Mammone, H. K. Mao, and P. M. Bell, Geophys. Res. Lett. **8**, 140 (1981).
[22]P. Richet, H. K. Mao, and P. M. Bell, J. Geophys. Res. **80**, 15279 (1988).
[23]L. G. Liu and W. Bassett, J. Geophys. Res. **78**, 8470 (1973).
[24]Y. Sato and R. Jeanloz, J. Geophys. Res. **86**, 11 773 (1981).
[25]R. A. Robie, B. S. Hemingway, and J. R. Fisher, U. S. Geological Survey Report No. 1452, 1978 (unpublished).
[26]I. Jackson and H. Neisler, in *High-Pressure Research in Geo-*

physics, edited by S. Akimoto and M. H. Manghnani (Center for Adacemic Publications, Tokyo, 1982), pp. 93–113.
[27]M. S. T. Bukowinski, Geophys. Res. Lett. **12**, 536 (1985).
[28]Y. Tsuchida and T. Yagi, Nature (London) **340**, 217 (1989).
[29]L. G. Liu, W. A. Bassett, and T. Takahashi, J. Geophys. Res. **79**, 1160 (1974).
[30]N. L. Ross, J. F. Shu, R. M. Hazen, and T. Gasparik, Am. Mineral. **75**, 739 (1990).
[31]M. Sugiyama, S. Endo, and K. Koto, Mineral. J. **13**, 455 (1987).
[32]J. D. Bass, R. C. Liebermann, D. J. Weidner, and S. J. Finch, Phys. Earth Planet. Inter. **25**, 140 (1981).
[33]M. S. Vassiliou and T. J. Ahrens, Geophys. Res. Lett. **8**, 729 (1981).
[34]R. Boehler, J. Geophys. Res. **86**, 7159 (1981).